Pergamon

PII: S0191–8141(98)00009–1

Journal of Structural Geology, Vol. 20, No. 6, pp. 727 to 743, 1998

0191-8141/98 $19.00 + 0.00

Use of microgranitoid enclaves as solid state strain markers in deformed granitic rock: an evaluation

O. T. TOBISCH and Q. WILLIAMS

Earth Science Department, A232 E. & M.S. Bldg., University of California, Santa Cruz, CA 95064, U.S.A.

(*Received* 8 *July* 1997; *accepted in revised form* 16 *January* 1998)

Abstract—Microgranitoid enclaves are common in many plutons and are potentially valuable as solid state strain markers in tectonically deformed granitoids. We consider the parameters necessary to assess enclaves as two-dimensional strain markers. These include (i) their primary shapes, (ii) differences in rheology between enclave and host granitoid, (iii) the magmatic shape fabric ellipse of enclave populations, (iv) the maximum fluctuation of enclave long axes developed during magmatic processes, (v) the angle between the magmatic shape fabric ellipse and tectonic strain ellipse at the onset of tectonic deformation, and (vi) the type of strain path undergone by the markers.

Enclave populations show characteristic magmatic distributions as shown by plots of the magmatic shape fabric ellipse vs enclave axial fluctuation from several plutons in the Sierra Nevada, California, and in the Adamello massif, Italy. The plots of tectonically *undeformed* and *deformed* enclaves show nearly complete overlap, creating substantial uncertainties in separating magmatic strain from tectonic strain if only the final enclave axial ratio is considered. Enclave/host strength differences have been modeled using published mineral deformation data and theoretical approaches to simulate deformation of aggregates. Results indicate very similar flow properties of enclaves and felsic host between 500° and 800°C, and possibly at lower temperatures as well, provided that biotite-bearing enclave and host compositions are present.

Two-dimensional strain modeling of the enclave populations indicates that values of the total shape fabric ellipse as determined from field measurements can be close to the true tectonic strain under some circumstances, but most commonly the former substantially over- or underestimates the latter. If the parameters (i–v) are assessed at each strain site, however, and each measured surface subsequently modeled using those parameters, over- and underestimates of solid state strain can be greatly reduced or eliminated, and reasonable values for two-dimensional tectonic strain of the granitoid and its enclaves can be obtained. © 1998 Elsevier Science Ltd. All rights reserved

INTRODUCTION

The state of solid state strain in granitic rocks may provide crucial constraints on regional tectonic strain patterns, or strains induced by local deformation. Quantitative studies of solid state strain in granitic rocks have been few, and for the most part have utilized various aspects of rock fabric or crystal shape/contiguity to estimate the symmetry and magnitude of the strain ellipsoid (e.g. Stauffer, 1967; Lacassin and van den Driessche, 1983; Schwerdtner, 1984; James *et al*., 1989). Although microgranitoid enclaves (henceforth referred to as enclaves) are a conspicuous feature of many plutons in orogenic belts, such enclaves have been studied mostly in the context of their field relations, petrologic and geochemical features, and their probable origin (e.g. Knopf and Thelan, 1905; Pabst, 1982; Didier, 1973; Vernon, 1983; papers in Didier and Barbarin, 1991); their structural utility as a quantitative solid state strain marker has been touched upon (e.g. Ramsay and Huber, 1983), but not thoroughly examined. Most structural usage of enclaves as strain markers has centered on magmatic or pre-full crystallization strain (Hutton, 1988a), that is, strain undergone by host and enclave magmas when there was melt present and in which evidence for solid state strain is largely absent (e.g. Holder, 1979; Hutton, 1988b; John and Blundy, 1993). Such strains are likely to occur during ascent and emplacement of the magmas, although the interpretation of strain results and their relation to emplacement history is currently under discussion (e.g. Paterson and Vernon, 1995). This paper focuses on the use of enclaves as markers for solid state strain imposed on an already crystallized granitoid (i.e. free of melt), either as it cools initially or is deformed at a later time synchronous with metamorphism under temperature conditions ranging from lower amphibolite to mid-granulite facies (i.e. 500°–800°C). Here, we examine trends in enclave shape from several plutons, consider aspects of their pre-solid state strain orientation, calculate the deformational properties of enclaves relative to their host, model some possible strain paths that produce deformed enclaves, and derive a set of criteria by which enclaves should be evaluated before being used as strain markers.

Our earlier work on enclave deformation (Williams and Tobisch, 1994) and this study focus on the 'end members' of the physical regimes in which enclaves can deform, that is, strain undergone by enclaves in the largely molten state (i.e. silicate melt > ~ 30%) and in the solid state (i.e. melt 0%), respectively. Although in some deformation environments such as syntectonic pluton emplacement, there is likely to be a continuum

between these 'end member' states, in others where time lapses occur between orogenic events, there is not a continuum. Additionally, enclave deformation in the submagmatic state (Paterson *et al.*, 1989), that is, with anywhere from trace amounts to ~30% melt present in enclave and/or host, is potentially a more complex problem, and a clear evaluation requires a separate treatment. In such situations, the geometric distribution of melt is likely to be of pivotal importance in determining the deformability of the aggregate. Hence, we think that there is greater clarity in evaluating the difficulties concerned by treating the different 'end members' separately.

FACTORS AFFECTING THE ACCURACY OF STRAIN MEASUREMENTS

The theoretical and practical methodology for quantifying strain in rocks has been treated by numerous workers (e.g. Ramsay, 1967; Elliott, 1970; Dunnet and Siddans, 1971; Ramsay and Huber, 1983; Lisle, 1985; De Paor, 1988). The main variables that affect the reliability of strain measurements are: (i) the primary shapes of the enclaves, (ii) the contrast in rheology between strain marker and its host, (iii) the magmatic shape fabric ellipse of enclave populations, (iv) the maximum fluctuation of enclave long axes developed during magmatic processes, (v) the angle between the magmatic shape fabric ellipse and tectonic strain ellipse, and (vi) the type of strain path (e.g. non-rotational strain, rotational strain, or some combination thereof) undergone by the marker. Although there are additional factors that can influence strain measurements, we consider (i)–(vi) above in assessing the utility of enclaves as solid state strain markers in granitic rocks. We restrict our analysis to aspects of two-dimensional strain, since enclaves are most commonly exposed on planar joint surfaces. Procedures for calculating a three-dimensional strain ellipsoid using two-dimensional enclave data are similar to those using other types of strain markers, and readers are referred to already published work (e.g. Oertel, 1970; Shimamoto and Ikeda, 1976; Miller and Oertel, 1979; Ramsay and Huber, 1983; Wheeler, 1986, and others). Since the size and distribution of enclaves preclude their accurate measurement under laboratory conditions, it greatly simplifies the steps in constructing the three-dimensional ellipsoid if the joint surfaces containing enclaves are parallel or nearly parallel to the principal planes of the strain ellipsoid at each site; otherwise more involved procedures such as outlined by some of the above authors may need to be applied.

In the following discussions, we refer to various geometrical features of the enclave populations in their tectonically undeformed and deformed states, and these are defined and illustrated in Fig. 1. Additionally, we mentioned that the type of strain path [item (vi), above] is an important factor, which may puzzle some readers, since the solid state strain of a homogeneous body is independent of the strain path and a function of the tensors of their pre-tectonic and

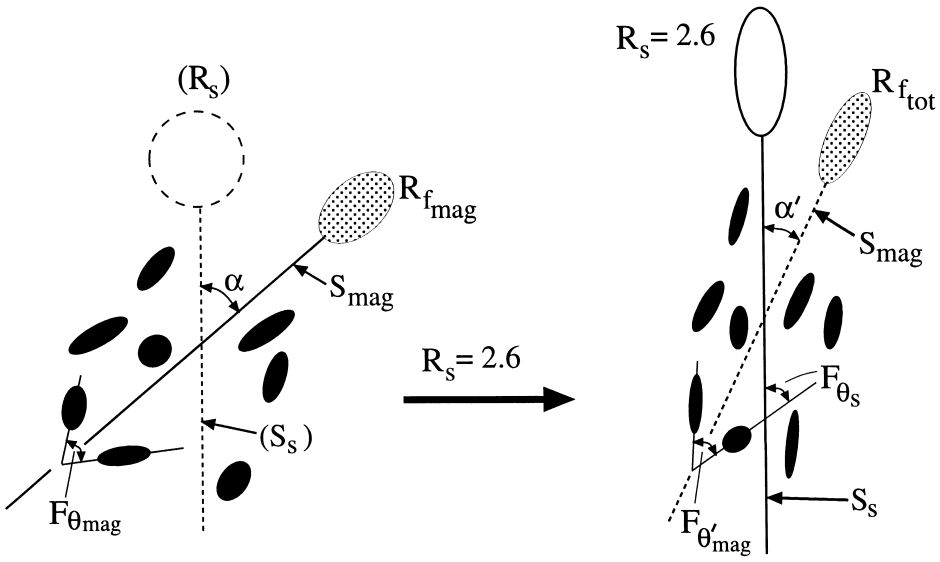

Fig. 1. Symbols of structural components of enclave populations used in text and figures as shown in their tectonically undeformed ($R_s = 1$) and deformed ($R_s = 2.6$) states. S_{mag}: magmatic foliation; S_s: solid state foliation; $R_{f_{mag}}$: final axial ratio of shape fabric ellipse (determined by R_f/ϕ) of enclave population developed *under magmatic conditions*; $R_{f_{tot}}$: as above except R represents axial ratio of total strain ellipse accumulated during both *magmatic and tectonic (solid state) components*; $F_{\theta'_{mag}}$ and $F_{\theta'_{mag}}$: angle of maximum fluctuation of enclave long axes in an enclave population before and after imposition of a tectonic strain (resp.) with angle θ measured to the S_{mag}; F_{θ_s}: as above *after* tectonic strain with angle θ measured to the S_s; α and α': angle between the S_{mag} and S_s before and after imposition of a solid state strain (resp.); R_s: axial ratio of tectonic strain ellipse imposed on enclave population; R_p: average primary shape ellipse of enclaves (see text for details).

tectonic strain states (e.g. Sanderson, 1976; Schwerdtner and Gapais, 1983). However, in the field one is restricted to determining the strain indirectly by measuring the shapes and orientation of the enclaves. Even though the total body may deform homogeneously and produce the same value of strain independent of the path, the enclaves will have different geometrical relations to the strain ellipse in each case and pass through different shape changes depending in part on whether the strain is rotational or non-rotational. Figure 2 illustrates that given the same starting configuration (Fig. 2a), the difference between the strain undergone by the homogeneous body (R_s) and that measured by the enclaves ($R_{f_{tot}}$) is substantially different contingent on whether the strain imposed is non-rotational (Fig. 2b) or rotational (Fig. 2c). This difference can be explained by considering that in the non-rotational case, most of the long axes of the enclaves lie in zone 1 of the deformation ellipse (Fig. 2d) and extend continuously during the deformation, whereas in the rotational case, many enclave long axes initially lie in either zones 2 and 3 (Fig. 2e) and start out contracting before rotating sufficiently to lie in the field of extension (cf. Ramsay, 1967, p. 114). Hence, even though R_s is the same in both paths, the final enclave axial ratios ($R_{f_{tot}}$) in the former (Fig. 2b) will be higher than in the latter (Fig. 2c), although it should be noted that with different angular relationships, the reverse could be the case. We consider this and other ramifications in more detail later in the paper.

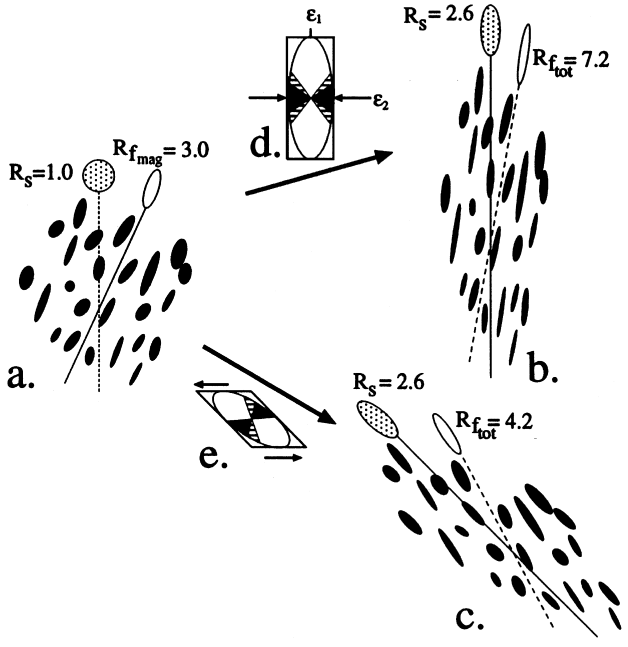

Fig. 2. Illustration showing how (a) an original population of enclaves with $R_{f_{mag}} = 3.0$, $F_{\theta_{mag}} = 50^\circ$ and $\alpha = 25^\circ$ subjected to non-rotational (b) and rotational (c) strain paths can give rise to different 'errors' between $R_{f_{tot}}$ and R_s even though the bulk strain has the same final value for both paths. (d) Progressive deformation ellipse for non-rotational strain (modified from Ramsay, 1967, figs 3-62 and 3-64) showing the three deformation zones: zone 1, no pattern, lines lengthen only; zone 2, horizontal stripes, lines shorten and then lengthen, and zone 3, black area, lines shorten only. Deformation ellipse was generated with $\varepsilon_1 = 160\%$ and $-\varepsilon_2 = 38\%$. (e) Similar to (d) but deformation ellipse generated by a rotational strain of $\gamma = 1$.

ORIGINAL ORIENTATIONS AND SHAPES OF ENCLAVES

Orientations

If markers initially show little preferred orientation within the host, the value of the shape fabric ellipse can be separated from the value of strain using the R_f/ϕ method (Ramsay, 1967). The presence of an initial fabric, however, introduces considerable error into the method. The unstraining procedures that were developed to correct this error are most effective (a) if specimens contain small markers and therefore can be precisely slabbed and analyzed in the laboratory (e.g. Elliott, 1970; Dunnett and Siddans, 1971), (b) if they contain a marker horizon (e.g. bedding), and (c) if the samples show a symmetric distribution about a mean direction (e.g. De Paor, 1988). Many rocks that bear non-random fabrics, such as massive volcanic lapilli tuffs and breccias, etc., contain strain markers that are too large, too widely dispersed, and/or lack the marker horizons necessary to carry out unstraining procedures in the laboratory (e.g. Ramsay and Huber, 1983). In such instances, determining initial shape distributions from undeformed protoliths may provide useful constraints in calculating values of strain (e.g. Tobisch *et al.*, 1977).

Enclaves in granitic plutons can show very low degrees of preferred orientation of their long axes. For example, magmatically deformed enclave populations from granitoids in the Adamello Massif analyzed by John and Blundy (1993) using the methods of De Paor (1988) suggested that enclaves at the majority of sites within this pluton showed little preferred orientation in the host granitoid prior to their pre-full crystallization strain. We observe that enclaves in plutons from the Sierra Nevada, California, commonly contain a subtle preferred orientation which is only visually apparent in R_f/ϕ diagrams. Figure 3 illustrates R_f/ϕ plots from two of the plutons which have igneous foliation varying from absent to moderately developed. There are subtle (e.g. Fig. 3a & b) to obvious (e.g. Fig. 3c) departures from symmetry of their enclave populations, indicating varying degrees of preferred orientation among the enclaves. As expected, where igneous foliation is stronger, the fluctuation ($F_{\theta_{mag}}$) of the enclave long axes becomes smaller ($\pm 20^\circ$), and an initial asymmetry that may have been present becomes occluded (Fig. 3d). Superposition of even a relatively weak solid state strain on the population shown in Fig. 3(d), for example, could yield an apparent symmetric distribution of enclaves in which it would be

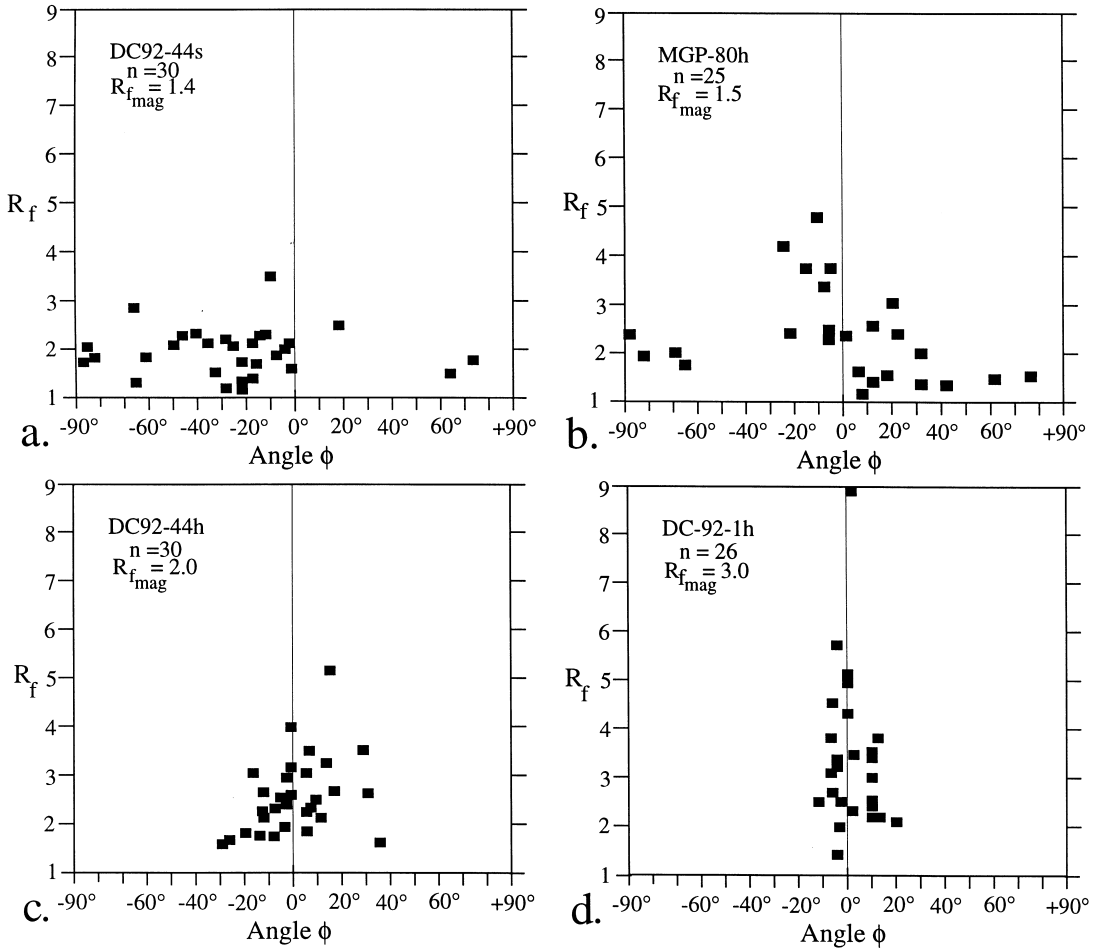

Fig. 3. R_f/ϕ diagrams of enclaves from the Dinkey Creek and Mt Givens plutons. (a–d) Rocks at these sites have not been subjected to solid state strain. DC = Dinkey Creek pluton, MGP = Mt Givens pluton, s = steeply dipping or h = subhorizontally dipping surfaces of measurement lying at high angles to the magmatic foliation (S_{mag}).

very difficult to separate initial shape from that imposed by tectonic strain.

In any event, pre-full crystallization strain of the granitic host and enclaves during ascent and emplacement will impose varying amounts of preferred orientation on the enclaves. Solid state strain during a subsequent tectonic event, therefore, will be imposed on enclave populations with a potentially wide range of axial ratios and degree of preferred orientation (e.g. Fig. 3a–d). It is important, therefore, to consider initial shape variations of enclaves.

Shapes

Most enclaves in granitic rocks form by the mingling of a mafic and/or intermediate enclave magma with a felsic host magma (Vernon, 1983). The mingling process is enhanced if the host magma is either flowing while the enclave magma is injected into it or begins flowing immediately thereafter. Depending on a range of dynamic factors, which include the rate of flow of the host, the volume of the enclave magma and its force of injection and the viscosity contrast between host and enclave, globules will separate from the enclave magma and form various shapes. Two principal mechanisms of enclave production in this magmatic deformation regime are tip streaming and fracturing or boudinage (Williams and Tobisch, 1994). Although initial enclave shapes can be roughly equidimensional (e.g. Vernon *et al.*, 1988, figs 2 and 3; John and Blundy, 1993, fig. 5a; Williams and Tobisch, 1994, fig. 1a), continuing shear produced during differential flow of the host usually modifies the enclaves into ellipse-like shapes (Fig. 4a); more irregular shapes can often be fit by an ellipse.

Two-dimensional enclave axial ratios and orientations can vary substantially over very short distances (Fig. 4b; see also Pabst, 1928, plate 46b and 47b). Different axial ratios in contiguous enclaves may result from variation of rates of magma flow in contiguous domains of the host, by bringing together enclaves formed in different parts of the host magma as different batches comingle, and through different solidification histories of chemically different enclaves. It is also likely that at least some examples of extreme variation (Fig. 4b) are an artifact of erosion. If the enclave has a complex shape, the view plane will sample only one cross-section through the complex shape, with the

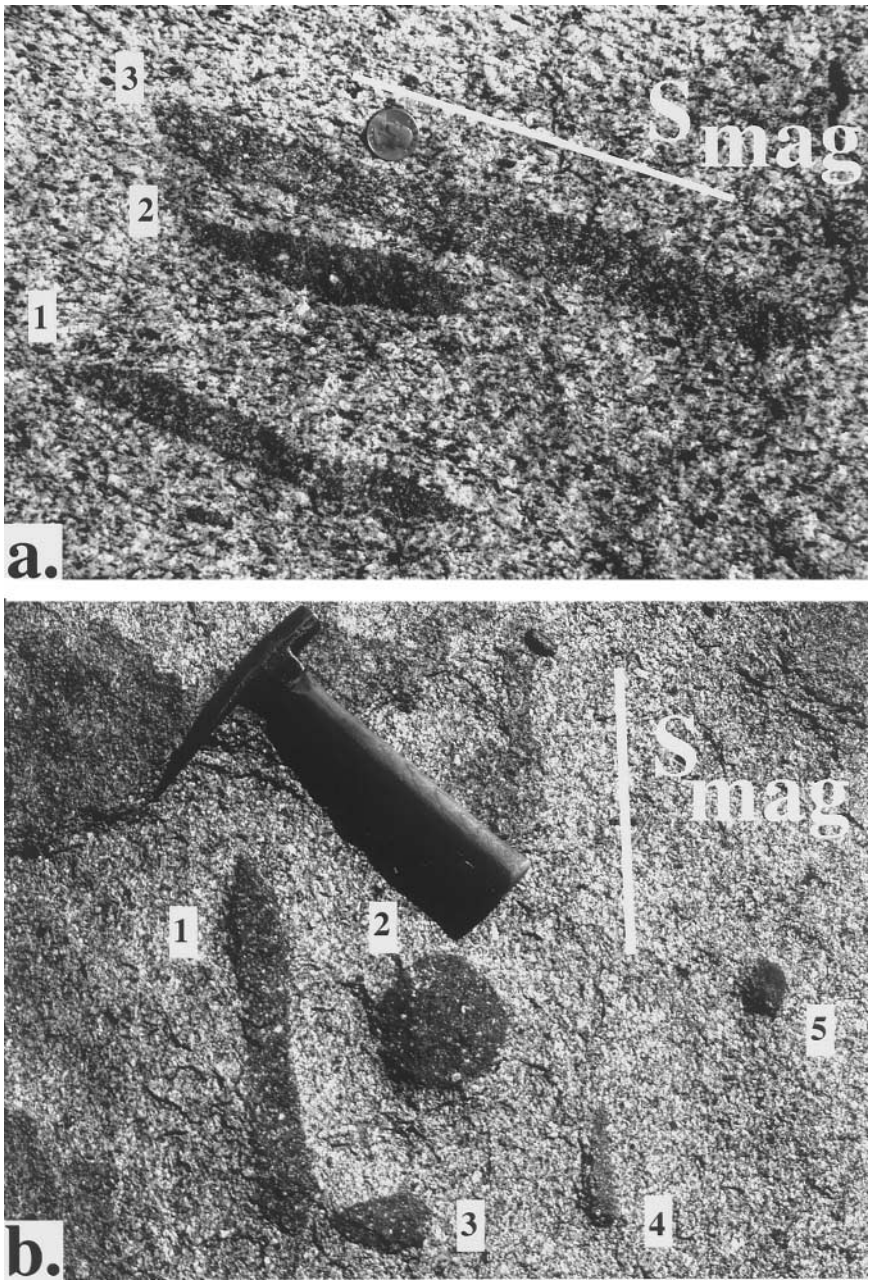

Fig. 4. Photographs of enclaves in the Dinkey Creek pluton, central Sierra Nevada, California. (a) Typical enclaves showing different composition and axial ratios that vary between 7.5:1 (top) to 3.5:1 (center). Magmatic foliation (S_{mag}) is moderately well developed. Photograph taken near Wishon Reservoir dam. Coin is 2.4 cm diameter. (b) Enclaves showing distinct compositional variation and substantial variations in axial ratio (7:1–1:1) and orientation (90°; see text for discussion). Magmatic foliation (S_{mag}) is weakly developed. Located just north of Dinkey Creek road, ~1.8 km southwest of where Stevenson Creek enters Shaver Lake. Hammer handle ~28 cm.

remainder lying beneath the observation surface (the tip-of-the-iceberg effect). Srogi and Lutz (1990) present evidence from slabbed and computer reconstructed mafic enclaves which suggest how different axial ratios and orientations of apparently separate enclaves could result from random cuts through one large and complexly shaped mass, with apparently separate enclaves being connected beneath the view plane. Figure 4(b) may illustrate such an occurrence. Enclaves 1–3 are closely spaced and compositionally similar, but are quite different from enclaves 4 and 5 in phenocryst or mafic mineral content. Enclaves 1–3 could represent prongs from a single irregular enclave which intersects the view plane as three apparently separate enclaves. In Fig. 4(a), on the other hand, enclaves 1–3 are all of different composition; although closely spaced, they thus probably represent separate, detached enclaves.

The point here is simply that contiguous, isocompositional enclaves which show extreme variations in ratios and/or orientations (e.g. Fig. 4b) will yield equivocal results if used as strain markers. Fortunately, it is more common to find only a modest percentage (~5–20%) of enclaves that show variation in axial ratios lying far off the norm (Fig. 5). Enclaves

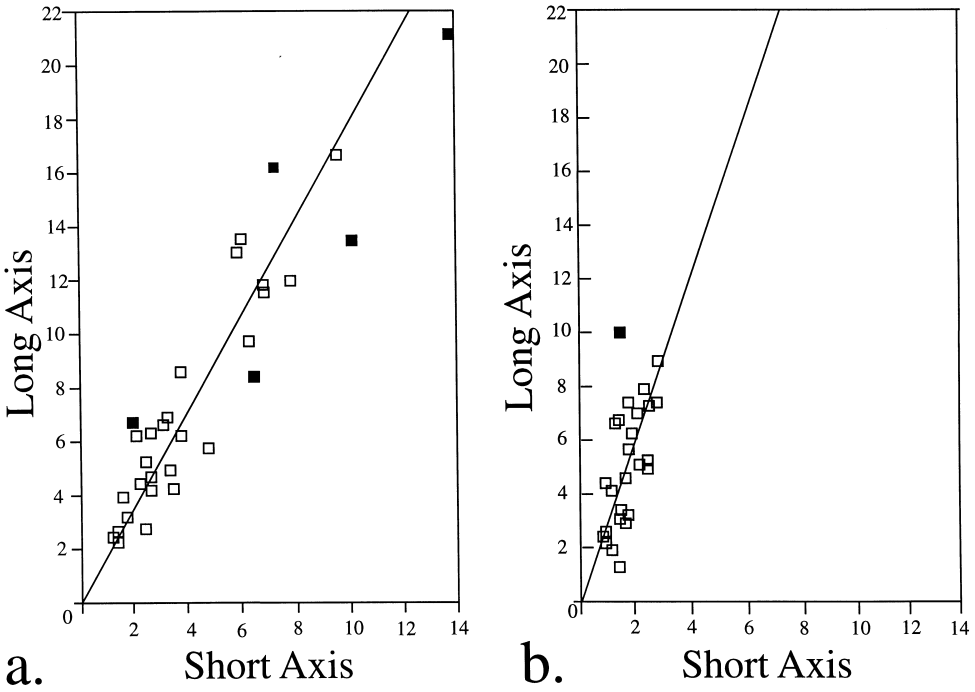

Fig. 5. Long–short plots of enclave axes from two stations in the Dinkey Creek pluton showing typical distributions. All measurements were made on surfaces essentially normal to S_{mag}. (a) Moderately well distributed plot exhibiting ~20% variance from main distribution. Black squares indicate enclaves with ratios significantly off main distribution. Measured surface dips very steeply. Sample size, $n = 30$; sample DC-92-44. (b) Relatively tight plot exhibiting ~4% variance from main distribution. Measured surface dips very gently. $n = 26$; sample DC-92-1.

in tectonically strained populations that may have had unusual initial axial ratios or orientations are often obvious, and if appropriate, may be eliminated from strain analyses. In most cases, the axial ratios of the remainder of the enclaves at any given site show sufficient internal consistency of initial shape to be used as valid strain markers (e.g. Fig. 5).

RHEOLOGIC DIFFERENCES BETWEEN ENCLAVE AND HOST

Although the effect of strength differences between generic marker and host was quantitatively investigated by Ramsay (1967) and Gay (1968a,b), the strength difference between enclaves and granitic host during deformation in the solid state has remained largely one of qualitative field observations. Choukroune and Gapais (1983, p. 416), working in deformed greenschist facies granitoids, assumed that this difference was small because of the "lack of significant refraction" of solid state foliation (S_s) across enclaves. In the Courtright shear zone, a moderately high temperature (~600–680°C) domain of deformation in granitoids (Tobisch *et al.*, 1993), enclaves do not show pressure shadows (Fig. 6a) and S_s in the host is parallel to S_s in the enclave (Fig. 6b). However, the Courtright enclaves are intermediate in composition, with biotite > hornblende, and may behave differently than amphibole-rich enclaves. To better constrain the level at which enclaves mirror the deformation of their host, we evaluated the potential rheologic contrasts between granitic rock and enclave using extant experimental data on mineral deformation, coupled with theoretical approaches designed to simulate the deformation of aggregates. These data allow us to explore rock rheologies over a limited range of temperatures from ~500°–800°C, corresponding approximately to temperature conditions found in lower amphibolite to mid-granulite facies metamorphism and their lower pressure equivalents (Turner, 1981). Our rationale for exploring the high end of this temperature range is primarily to compare the rheologic behavior of enclaves and hosts under reasonably dry granulite facies conditions. At temperatures of near 800°C under fluid absent conditions, amphibolite assemblages retain their solid-state strength without the onset of melt-induced weakening (Rushmer, 1995), while the amount of melt present in granites under these conditions is only 3% (Rutter and Neumann, 1995). Therefore, our solid-state modeling approach should be applicable to fluid absent conditions for both hosts and enclaves at temperatures between 750–800°C.

Modeling approach

To calculate the rheologic properties of mafic and granitic aggregates of various mineralogies at sub-solidus conditions, we utilize the algorithm of Tullis *et al.* (1991) coupled with single phase flow laws for plagioclase, quartz, biotite and amphibole. This method of calculating aggregate rheologic properties depends pri-

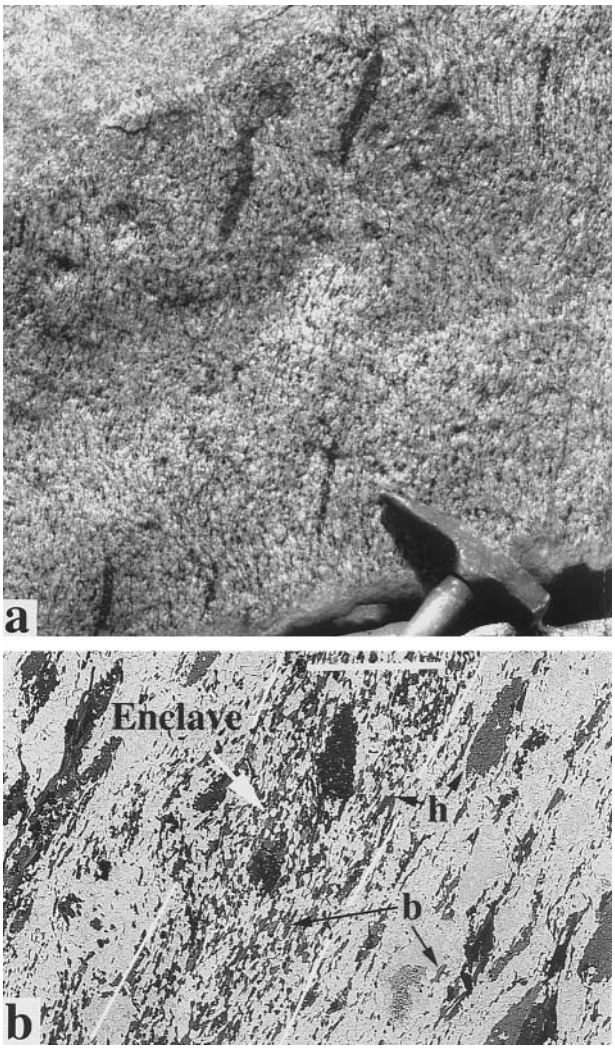

Fig. 6. (a) Strongly deformed Dinkey Creek tonalite in the Courtright shear zone as seen on a vertical joint face ($\sim XZ$ section). Although the solid state foliation (S_s) is affected by weak shears (dipping gently to the right) which warp it, enclaves appear to lie very closely to S_s. Note the similarity of enclave axial ratios, and the lack of pressure shadows on the enclave ends. Hammer head is ~35 cm. (b) Photomicrograph in plain polarized light of tonalitic host and enclave microfabric in a sample from an exposure a short distance from (a), illustrating the continuity and parallelism of foliation between them. b = biotite, h = hornblende. Width of white scale bar at top of photo is 0.6 cm.

marily on the volume fraction of the phases present, and assumes that the flow law of an aggregate represents a geometric mean between the flow laws of the end members. The averaging technique has been found to yield aggregate rheologies which agree well with the results of finite element simulations of deformation of two-phase aggregates (Tullis *et al.*, 1991): its primary limitation involves its inability to model systems in which a rheologically weak phase is present on shear planes. This approach also incorporates the implicit assumption that dislocation creep predominates throughout the temperature range of our simulations, and thus we use single phase (and aggregate) flow laws of the form

$$\dot{\varepsilon} = A\sigma^n \mathrm{e}^{-Q/RT} \tag{1}$$

where $\dot{\varepsilon}$ is the strain rate, σ is the differential flow stress, n is the stress exponent, Q denotes the activation enthalpy for flow, T is temperature and R is the gas constant. Our assumption that dislocation creep predominates in these systems means that our analysis provides an upper limit on the flow stress at extremely high strain rates in these systems, where grain-boundary sliding, grain-boundary diffusion creep and cataclastic flow may become important (Tullis and Yund, 1985, 1987). These grain-size dependent flow regimes, for which few rheologic data exist, are thus not treated in our approach.

In order to determine the flow laws of three phase aggregates, we use a generalization of the equations of Tullis *et al.* (1991). Specifically, the stress exponent of the aggregate (n_a) is equal to

$$n_a = 10^{(f_1 \log n_1 + (f_2+f_3)\log[(f_2/(f_2+f_3))\log n_2 + (f_3/(f_2+f_3))\log n_3])} \tag{2}$$

in which $f_{1,2,3}$ denote the volume fractions of the three phases and $n_{1,2,3}$ are the stress exponents of each individual phase. Accurate averaging is achieved by assessing equation (2) with differing subscripts assigned to each phase: characteristic differences in stress exponents of less than 0.03 are produced between different averaging schemes. Such differences are negligible in comparison with experimental uncertainties in the flow laws, and we thus conclude that the order in which phases are incorporated into the averaging equations does not influence our results. The activation enthalpy (Q_a) for the assemblage in this averaging scheme is

$$\begin{aligned} Q_a = &[[(Q_2(y-n_3) - Q_3(y-n_2))/(n_2-n_3)] \\ &(n_a-n_1) - Q_1(n_a-y)]/(y-n_1) \end{aligned} \tag{3}$$

where $Q_{1,2,3}$ are the respective activation enthalpies of each phase, and y is the quantity in brackets in equation (2). Similarly, the pre-exponential factor in the flow law of the aggregate (A_a) is

$$\begin{aligned} \log A_a = &[(n_a-n_1)[[(y-n_3)\log A_2 - (y-n_2)\log A_3]/ \\ &(n_2-n_3)] - (n_a-y)\log A_1]/(y-n_1) \end{aligned} \tag{4}$$

in which $A_{1,2,3}$ are the pre-exponential factors in the flow laws of each phase. This method for averaging the rheologic parameters of a polyphase aggregate is generally compatible with the technique of Handy (1990) which is derived from the additivity of the strain energy (and strain rate) expended on each constituent being equivalent to the sum of the strain energy for each constituent of a rock. Both the approach of Tullis *et al.* (1991) and Handy (1990) produce flow laws for rocks which are intermediate between those of their end-member components, and which depend on the volume fraction of minerals within rocks and geometric averaging of the end-members' rheologic parameters.

We calculate the dependence of rheology on temperature for differing host and enclave mineralogies

using equation (1) by both assuming constant strain rates of 10^{-13}/s, in approximate accord with inferred deformation rates in moderately fast strain zones (Pfiffner and Ramsay, 1982; Paterson and Tobisch, 1992), and for the higher strain rates (10^{-11}/s) expected in mylonite zones (Schmid, 1989). Additionally, we calculate strain rates for differing mineralogies for constant imposed stresses of both 10 MPa and a higher stress (again, possibly associated with mylonite zones) of 100 MPa. Our single-phase rheologies for feldspar are derived from the flow law derived by Shelton and Tullis (1981) from measurements conducted between 650°C and 1125°C, and quoted by Tullis *et al.* (1991): because of the abundance of feldspar within both mafic enclaves and host materials, our simulations are most sensitive to the flow law of this material. In detail, the flow laws for albite and anorthosite are nearly indistinguishable, although that of albite is considerably better constrained (Shelton and Tullis, 1981); as a result, we do not anticipate that the detailed chemistry of plagioclase will significantly impact its flow properties. No measurements are available on the flow law of single phase amphibole: however, Hacker and Christie (1990) conducted solid-state rheologic measurements on a well-characterized amphibolite assemblage with a mineralogy of 53% amphibole, 43% plagioclase, and 4% trace phases. From the aggregate averaging technique of Tullis *et al.* (1991) coupled with the flow law for plagioclase of Shelton and Tullis (1981), we are able to extract a flow law for end-member amphibole from the amphibolite deformation data. This derived amphibole flow law has a pre-exponential factor (A) of 5.1×10^{-3}s/(MPa)$^{-n}$, an activation enthalpy of 254 kJ/mol and a stress exponent of 3.5. It is notable that both the activation enthalpy and stress exponent of this flow law are similar to those of plagioclase: 234 kJ/mol and 3.9, respectively (Shelton and Tullis, 1981). Therefore, *the temperature dependence of amphibole strength is extremely similar to that of feldspar*. For quartz, we utilize rheologic flow laws derived from measurements on Heavitree quartzite under both dry and wet (0.4 wt% water) conditions (Kohlstedt and Evans, 1995); for biotite, the basal flow law of Kronenberg *et al.* (1990) is utilized.

Our characteristic mineralogies of the host are: 60 vol.% feldspar, 20 vol.% quartz, and 20% of either amphibole or biotite; we assess the rheologies of the host using both dry and wet quartz, with our lower bound on the viscosity of the host being derived from a biotite-bearing assemblage with a wet quartz flow law, and our upper bound being produced from an amphibole-bearing assemblage with a dry quartz rheology. Enclave modes are assumed to vary between the mineralogy of a standard amphibolite (50% amphibole and 50% feldspar) and the approximate mineralogy of an enclave of intermediate composition (50% feldspar, 25% amphibole, and 25% biotite). The comparatively similar flow laws of amphibole and feldspar produce similar temperature dependences of the rheology of amphibolite and the upper bound on our host rheology (Fig. 7). As biotite and (to a lesser extent) quartz have differing temperature dependences from amphibole and feldspar, the calculated flow stress of the intermediate composition enclave is more similar to that of the lower bound on flow stress of the host: this similarity is generated by the comparable volumetric percentage of biotite in each assemblage. The general similarity of rheology between enclaves and hosts is reemphasized by our calculations of strain rates of differing aggregates at constant stress (Fig. 7c & d): the strain rates at a given stress are nearly indistinguishable at high temperatures and low stresses. Indeed, the large measured stress exponent for biotite ($n = 18$) produces a similar strain rate between the biotite-bearing and amphibole-bearing assemblages at stresses of 10 MPa and below.

From this analysis, we conclude that where the enclave and host compositions are similar, such as a biotite-bearing intermediate composition enclave (Fig. 7a, curve 3) occurring in a wet, biotite-bearing granitic host (curve 4), the rheologic differences at strain rates of 10^{-13}/s will be negligible. The strain recorded by the enclave, therefore, will be essentially the same as that present in the host, given the margin of error present (Fig. 7b): therefore, we expect that the magnitude of strain undergone by an enclave under these conditions should provide an accurate representation of the deformation within its host. Moreover, the rheologies of enclaves and host deformed under granulite facies temperatures should be similar at moderate strain rates and stresses irrespective of their compositions (Fig. 7a & c).

At the low end of lower amphibolite facies temperatures (~500°C), composition may potentially play a role in producing some difference in rheology between enclave and host, but only if the enclave mafic mineral phase is almost entirely amphibole (curve 1, Fig. 7a) and the granitic host is a wet, biotite-bearing rock (curve 4, Fig. 7a). In this case, a difference in flow stress of half an order of magnitude is possible at constant strain rate, and the enclave strain may record only a minimum strain value relative to that experienced by the host. If the curves at their present slopes are projected to temperatures typical of the greenschist facies (i.e. ~300°–500°C), we speculate that the difference in flow stress between the enclave and host shown by curves 3 and 4 (Fig. 7) will still be negligible, but for other compositional combinations (e.g. curves 1 and 4, Fig. 7a), the difference may increase to as much as an order of magnitude, although the rheologic data do not extend to sufficiently low temperatures to confirm this trend. A comparable difference in rheology between host and enclave at higher strain rates (10^{-11}/s, Fig. 7b) in the temperature range below 500°C is also possible.

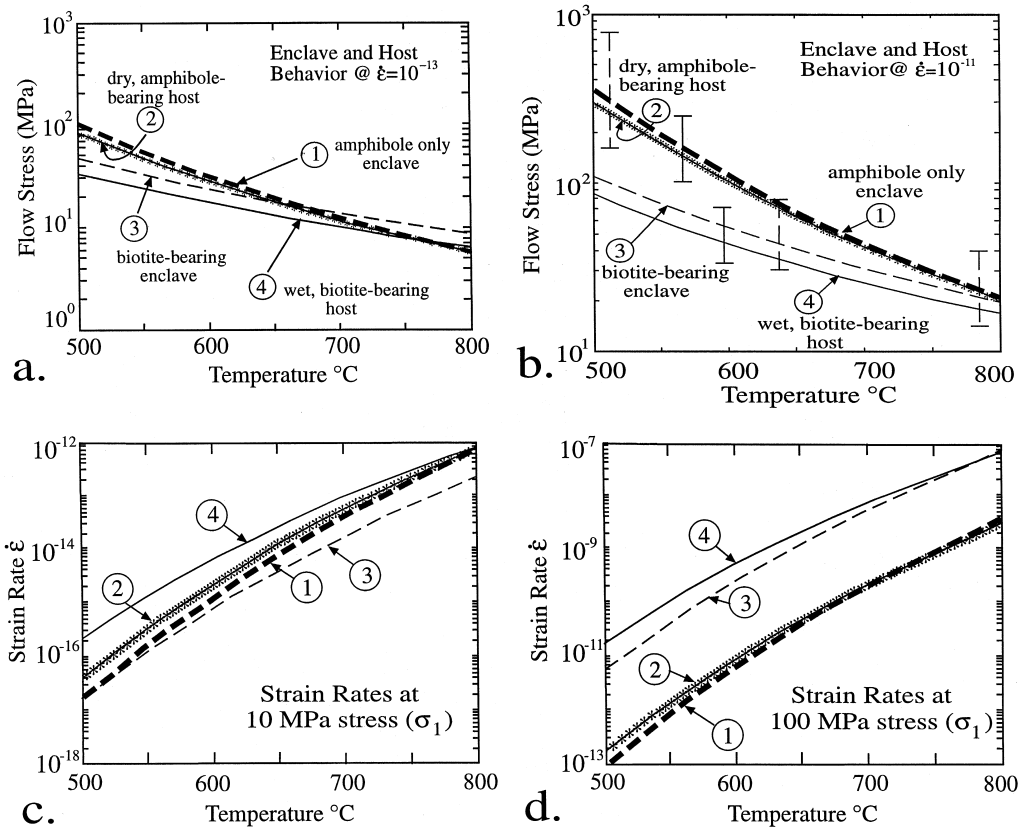

Fig. 7. Dependence of flow stress (at constant strain rate) on temperature and strain rate (at constant flow stress) for two host and two enclave mineralogies designed to provide limits on enclave and host rheologies. Heavy and light dashed curves correspond to amphibole only- and biotite-bearing enclaves, respectively; solid curves with and without asterisk pattern correspond to dry (no water within quartz) and wet (0.4 wt% water in quartz) amphibole- and biotite-bearing hosts, respectively. Error bars are calculated using standard error propagation techniques and are of similar magnitude in both (a) and (b). However, only errors on the pre-exponential factor in equation (1) have been reported for feldspar (Shelton and Tullis, 1981). Thus, the calculated error bars for these feldspar-rich assemblages are significantly asymmetric, and are relatively independent of temperature. Error bars in (c) and (d) scale as the error bars in flow stress, raised to the n power [see equation (1)]. (a) Strain rate = 10^{-13}/s. (b) Strain rate = 10^{-11}/s. (c) Stress (σ_1) = 10 MPa. (d) Stress (σ_1) = 100 MPa.

In summary, rheologic differences between enclave and host are negligible in upper amphibolite and granulite facies rocks at stresses near 10 MPa. At lower temperatures, some differences in rheology between host and enclave are possible when certain compositional and/or stress–strain rate situations are met (Fig. 7a–d). Similarly, for high stress situations such as occur within ultramylonite zones, major mineralogic differences between enclave and host [such as the case of an amphibole-bearing enclave (curve 1) contained within a biotite-bearing host (curve 4)], can produce significant differences in rheologic behavior (Fig. 7d). Accordingly, for deformation of enclave/host with significant compositional differences and occurring at comparatively low temperatures (greenschist facies) or high stresses (ultramylonite zones), one should be aware that there could be significant differences in rheologic properties between hosts and enclaves: such differences could prospectively bias inferred values of strain derived from enclaves which have been deformed under these conditions.

RELATIONS BETWEEN SHAPE FABRIC ELLIPSE ($R_{\mathrm{F}_{\mathrm{mag}}}$), ENCLAVE FLUCTUATION ($F_{\theta_{\mathrm{mag}}}$) AND STRAIN ELLIPSE ($R_{\mathrm{S}}$)

The last factors we consider are the values of the shape fabric ellipse ($R_{\mathrm{f}_{\mathrm{mag}}}$) and fluctuation of the enclaves ($F_{\theta_{\mathrm{mag}}}$) within a given population, and the result of imposing R_{s} upon $R_{\mathrm{f}_{\mathrm{mag}}}$ at differing values of angle α (see Fig. 1).

Range of ($R_{\mathrm{f}_{\mathrm{mag}}}/F_{\theta_{\mathrm{mag}}}$) enclaves in tectonically undeformed rocks

Cloos (1947) and Ramsay (1967) demonstrated that the degree of preferred alignment of markers in any population is a function of the ellipticity of the marker and the magnitude of the imposed strain, and this can be expressed in terms of the fluctuation. In Fig. 8, we plot data from tectonically undeformed enclave populations measured on 148 surfaces from several Sierra Nevada plutons. These data were plotted in terms of

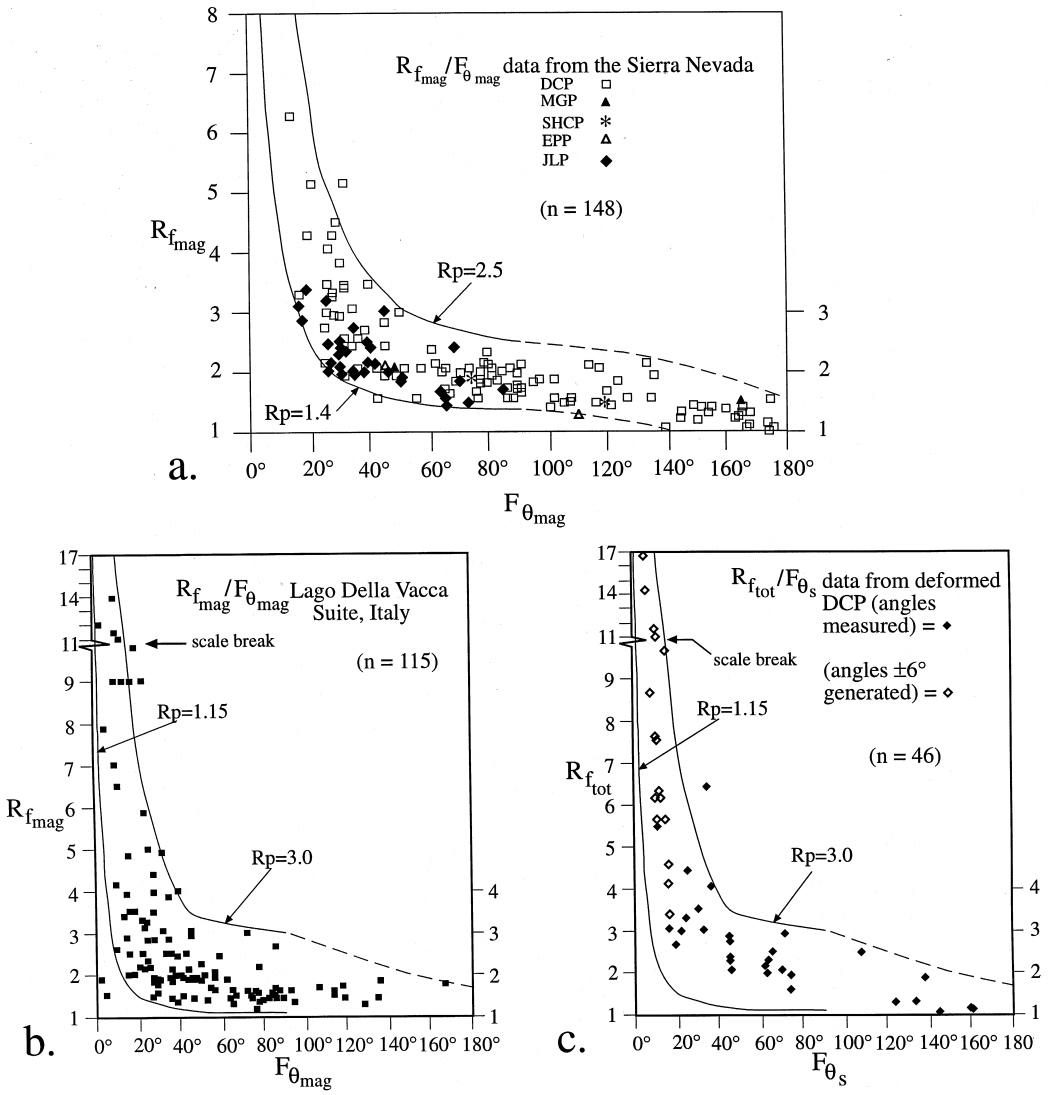

Fig. 8. $R_{f_{mag}}/F_{\theta_{mag}}$ plots from several plutons in the Sierra Nevada, California, and the Adamello massif, northern Italy. Symbols explained in Fig. 1. (a) Data from central Sierra Nevada, California: DCP = Dinkey Creek, MGP = Mt Givens, JLP = Jackass Lakes (Tong, 1994; W. Tong, written communication, 1997; McNulty *et al.*, 1996), SHCP = Short Hair Creek, and EPP = Eagle Peak plutons. $R_{f_{mag}}$ calculated using procedures of Shimamoto and Ikeda (1976). (b) Data from the Lago Della Vacca intrusive suite, Adamello massif, northern Italy (John and Blundy, 1993; B. John, written communication, 1997). Strain calculated using the procedures of De Paor (1988). See text for discussion. (c) Data from deformed domains of the DCP, Sierra Nevada, California; closed diamonds indicate angular data (ϕ) measured in field; open diamonds, angular data not measured in field but estimated during strain analysis assuming small values of ϕ ($\pm 6^\circ$) visually observed in field; details given in Tobisch *et al.*, 1993.

$R_{f_{mag}}/F_{\theta_{mag}}$, that is, the shape fabric ellipse ($R_{f_{mag}}$) at each site vs the maximum angular fluctuation ($F_{\theta_{mag}}$) of enclave long axes for that measured enclave population (Fig. 8a). The variation of $R_{f_{mag}}/F_{\theta_{mag}}$ values is considerable, and straddles a range that might be expected for markers recording very weak to moderately strong solid state deformation. The rocks at the measured sites display magmatic microstructures with only some weak minerals (quartz, biotite) locally modified by slight solid state deformation, a feature considered to be due to late-stage emplacement-related strain (cf. Bateman, 1992).

In Fig. 8(b), we plot the same parameters from 115 surfaces recorded from the Lago Della Vacca suite in the Adamello massif, Italy (John and Blundy, 1993). These data show even more variation than the Sierra Nevada data, recording strains of $R_{f_{mag}} \geq 10$ at a number of sites (Fig. 8b). John and Blundy (1993) and John and Stünitz (1997) find no evidence for active regional tectonic deformation during the emplacement, and consider strains in the Lago Della Vacca enclave suites to be entirely magmatic.

Interestingly, the results from the Sierra Nevada and the Adamello massif are very similar at lower strains ($R_{f_{mag}} < 6$), with the Lago Della Vacca data showing a greater number of higher $R_{f_{mag}}$ values than the Sierra Nevada data (Fig. 8a & b). Additionally, the Lago Della Vacca data set (below $R_{f_{mag}} < 4$) appear shifted slightly to the left, indicating a tendency towards lower strain/lower fluctuation than the Sierra Nevada popu-

lations. The data in Fig. 8 can be accurately bounded by a synthetic calculation using the dependence of angular fluctuation on the magnitudes of two shape-forming processes: the average primary shape ellipse (R_p) of enclaves as they were generated during magma mingling, and a secondary shape ellipse ($R_{f_{mag}}$) generated as the enclave populations take up strain during subsequent magmatic processes; the latter ellipse is most immediately relevant to solid state strain analysis. We utilize the algorithm of Ramsay (1967) to generate our synthetic bounds on the data of Fig. 8, in which

$$F_{\theta_{mag}} = \tan^{-1}[(R_{f_{mag}}(R_p^2-1))/((R_{f_{mag}}^2R_p^2-1)(R_{f_{mag}}^2-R_p^2))^{0.5}] \quad (5)$$

We suggest that the bounding curves of Fig. 8(a)($R_p = 1.4$–2.5) and 8(b)($R_p = 1.15$–3.0) may be a reflection of the major mechanisms which produced the enclaves (Williams and Tobisch, 1994), with tip streaming generating more equidimensional shapes (lower R_p) and fracturing/boudinage mechanisms during initial calving of magma globs producing enclave populations with higher ratios (higher R_p). That these mechanisms may occur to different degrees in the two pluton environments may reflect different magmatic temperatures during the magma mingling process, or may represent subtly different average enclave or host compositions between the two pluton suites. Although slight shift in enclave $R_{f_{mag}}/F_{\theta_{mag}}$ plots might be expected between plutons in different environments, we speculate that the enveloping curves shown in Fig. 8 ($R_p = 1.15$–3.0) may closely constrain the general distribution of enclave $R_{f_{mag}}/F_{\theta_{mag}}$ patterns found in most plutons.

One of the Sierra Nevada plutons studied, the Dinkey Creek pluton, contains domains of solid state strain, most notably the Courtright shear zone (Tobisch *et al.*, 1993); 46 enclave populations in those domains have been plotted separately (Fig. 8c), and show substantial overlap of $R_{f_{tot}}/F_{\theta_s}$ values (see Fig. 1 for definitions) with enclaves at tectonically *undeformed* sites from both the Sierra Nevada plutons and at Lago Della Vacca. Such overlap emphasizes one of the hazards of using enclaves for solid state strain markers: separating tectonically-induced solid state strain from the suite of possible magmatically-induced strains based on $R_{f_{tot}}/F_{\theta_s}$ data alone is subject to very large uncertainties.

Effect of angle between $R_{f_{mag}}$ and R_s (angle α)

Two factors that will further influence the final ratio and orientation of enclave populations that have been tectonically deformed are the angle (α) between $R_{f_{mag}}$ and R_s (Fig. 1) and the degree to which non-rotational strain, rotational strain or some combination thereof have acted on the enclaves (Fig. 2). The general effect of both these factors on strain markers has been known for some time (Ramsay, 1967). We briefly examine them in the context of enclaves, to elucidate under what conditions enclaves could be used as strain markers, and to emphasize both visually and quantitatively how differing strain paths and changes in the angles between, and magnitudes of, two different ellipses (i.e. $R_{f_{mag}}$ and R_s) can affect the values of the final enclave shape ellipse ($R_{f_{tot}}$) and R_s. The strain paths modeled assume no volume change and that enclave and host have the same strengths, as is consistent with our rheologic calculations (Fig. 7).

Figure 9(a) models a population of markers subjected to non-rotational strain with $R_{f_{mag}} = 2.6$, $\alpha = 25^\circ$, and $F_{\theta_{mag}} = 50^\circ$. When the strain on this path is increased to $R_s = 5.2$ (path I, Fig. 9c), the corresponding value of $R_{f_{tot}}$ is 13.5, nearly 260% the value of the tectonic strain R_s imposed. If the parameters are changed to $R_{f_{mag}} = 1.9$, $\alpha = 50^\circ$, and $F_{\theta_{mag}} = 85^\circ$, the path is similar, but the values of R_s (5.2) and $R_{f_{tot}}$ (6.0) are closer (path II, Fig. 9e), lying within ~12% of one another. However, when angle α is high, the path becomes retrograde for part of its 'journey' (path III, Fig. 9d & e), and $R_{f_{tot}}$ (2.6) records only ~50% of the final value of R_s (5.2). Notably, all the paths described fall within the 1.4–2.5 boundaries delineated by the undeformed populations of Fig. 8(a). Therefore, in two out of the three cases shown, the absolute value of $R_{f_{tot}}$ would appear to be a poor indicator of R_s.

In a rotational strain (Fig. 10a–d), with $R_{f_{mag}} = 1.9$, $\alpha = 45^\circ$, and $F_{\theta_{mag}} = 85^\circ$, the path veers out of the boundaries (path Ia, Fig. 10e) as a result of one enclave (A in Fig. 10) that increases the $F_{\theta_{mag}}$. If that enclave is eliminated from the analysis, however, the path stays within the boundaries (path Ib, Fig. 10e). More importantly, the final value in both subpaths is of $R_{f_{tot}} = 3.7$, recording only 75% of the strain ($R_s = 4.9$). With $R_{f_{mag}} = 2.6$, and $\alpha = 20^\circ$ and $F_{\theta_{mag}} = 35^\circ$ (path II, Fig. 10e), the value of $R_{f_{tot}}$ (13.4) overestimates the value of the true tectonic strain ($R_s = 4.8$) by nearly 280%.

Since many shear zones in transpressional orogens are a combination of non-rotational and rotational strains, we also modeled two combinations of those types of deformation in different sequences, since they are non-commutative (Ramsay, 1967). As illustrated in Fig. 11(a) and (b), which utilize varying parameters, paths I, II and III result in strikingly different values of $R_{f_{tot}}$ and R_s: path I shows $R_{f_{tot}} > R_s$ at 120%, and paths II and III show $R_{f_{tot}} \gg R_s$ at ~250% and 207%, respectively. Using different parameters in path IV (Fig. 11b), however, yields values of $R_{f_{tot}}$ and R_s that are very close, within 4%–8%. It is clear that given certain values of $R_{f_{mag}}$, angle α, and $F_{\theta_{mag}}$ (path IV, Fig. 11b) and combinations of rotational ($\gamma = 0.85$) followed by non-rotational strains (20% + 30% flattening), enclaves can yield relatively accurate estimates of tectonic strain. Knowing when those parameters hold, however, is a substantial uncertainty unless one

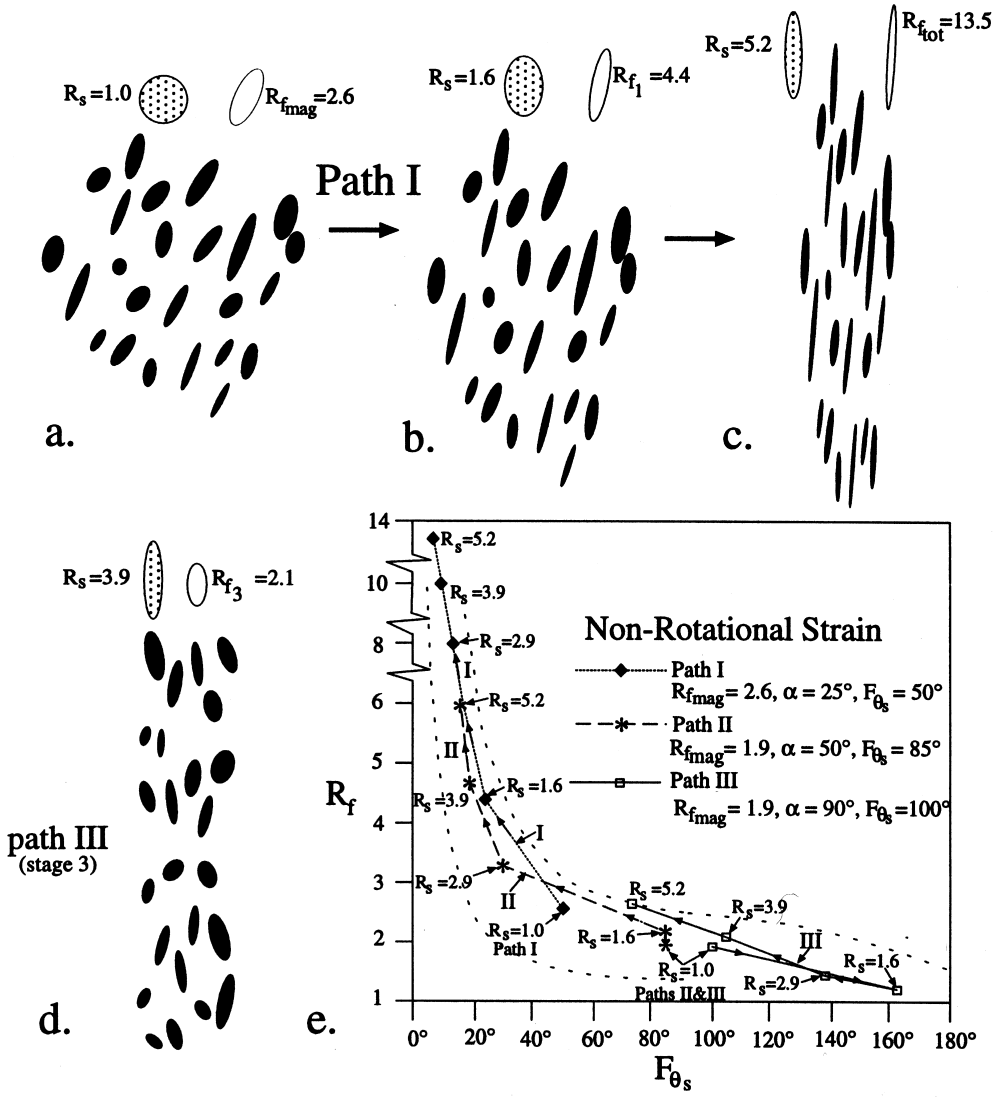

Fig. 9. Modeling of progressive non-rotational strains on a population of enclaves with given values of $R_{f_{mag}}$, $F_{\theta_{mag}}$, and angle α; see Fig. 1 for explanation of symbols. Dotted bounding lines are R_p boundaries taken from Fig. 8(a). (a–c) Deformation path I showing developing enclave fabric and differences in values of R_s and $R_{f_{tot}}$ at each stage, and the consistent relation of $R_{f_{tot}} > R_s$. R_{f_1} refers to intermediate value of R of the enclave population at the first stage in the progressive deformation shown in (e). (d) Third stage (R_{f_3}) of deformation path III [see (e)], showing reverse relation where $R_{f_{tot}} < R_s$. (e) Figure showing the three deformation paths I–III carried out under the different parameters shown. See text for details.

has excellent field observations to constrain their values and the sequence of strain events.

The significance of these data and simulations is that they show that (i) based strictly on the values of $R_{f_{tot}}$, enclave populations that have been subjected to relatively low tectonic strains ($R_s < R_{f_{tot}}$) fall within the same realm as, and are superficially identical to, tectonically undeformed enclave populations; (ii) with some (uncommon) exceptions, values of $R_{f_{tot}}$ in tectonically deformed enclave populations significantly over- or underestimate the true value of R_s; and (iii) although it may be difficult to estimate the initial (pretectonic) parameters at every site based on what field parameters are available, modeling the deformation process (e.g. Figs 9–11) can substantially constrain the final result of R_s. We discuss some guidelines below as to the conditions under which the magnitude of solid state strain in plutons can be optimized.

DISCUSSION AND CONCLUSIONS

From the above, it is clear that there are several initial parameters which affect the final value of $R_{f_{tot}}$ that one measures in the field. These initial parameters are: (i) strength contrasts between marker and host, (ii) angle α, (iii) $R_{f_{mag}}$, and (iv) $F_{\theta_{mag}}$. It is often possible by careful field observations at each field site to approximately reconstruct these initial parameters. One can then use these parameters to model which strain histories readily reproduce the final parameters measured in the field, i.e. $R_{f_{tot}}$, F_{θ_s}, and angle α'. This modeling process is greatly

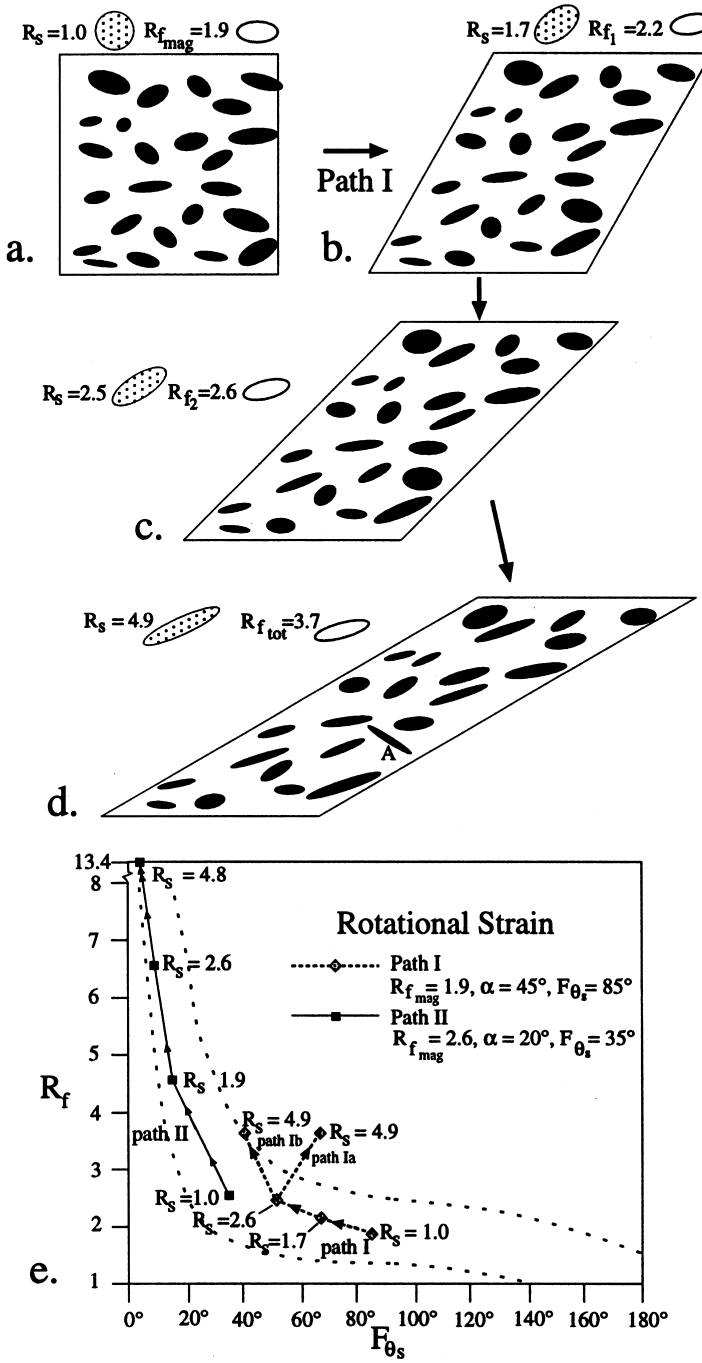

Fig. 10. Modeling of progressive rotational strains on a population of enclaves with different parameters as given in the figure. See Figs 1 and 9 for definition of symbols. The figure shows two possible deformation paths and condition sets.

facilitated by using widely available commercial graphics software (we used Macromedia Freehand, version 7.0), which provide transformation functions allowing rapid generation of results such as are shown in Figs 9–11. To set up the modeling, populations of ~25–30 enclaves with given values of $R_{f_{mag}}$ and $F_{\theta_{mag}}$ can be generated relatively easily with the graphics tools provided, forming a number of templates with possible 'initial states'. The different stages of progressive strain (e.g. in increments of $-\varepsilon_2 = 10\%$, or $\gamma = 0.05$) can also be set up easily, forming a second set of templates (care should be taken to ensure that equal area is maintained during the progressive stages). Differing parameters of imposed strain (R_s) and (α) such as are illustrated in Figs 1 and 9–11 can then be imposed on these initial state templates. By changing the various initial parameters in each 'run', one can quickly narrow the modeling results to approach the final values of $R_{f_{tot}}$, F_{θ_s}, and angle α' that one has measured at the strain site. Of course, the potential error may be largely contingent on the availability (and accuracy) of certain field parameters. We now briefly summarize the parameters used in the modeling to bring attention to the types of data that are useful to record at each field site.

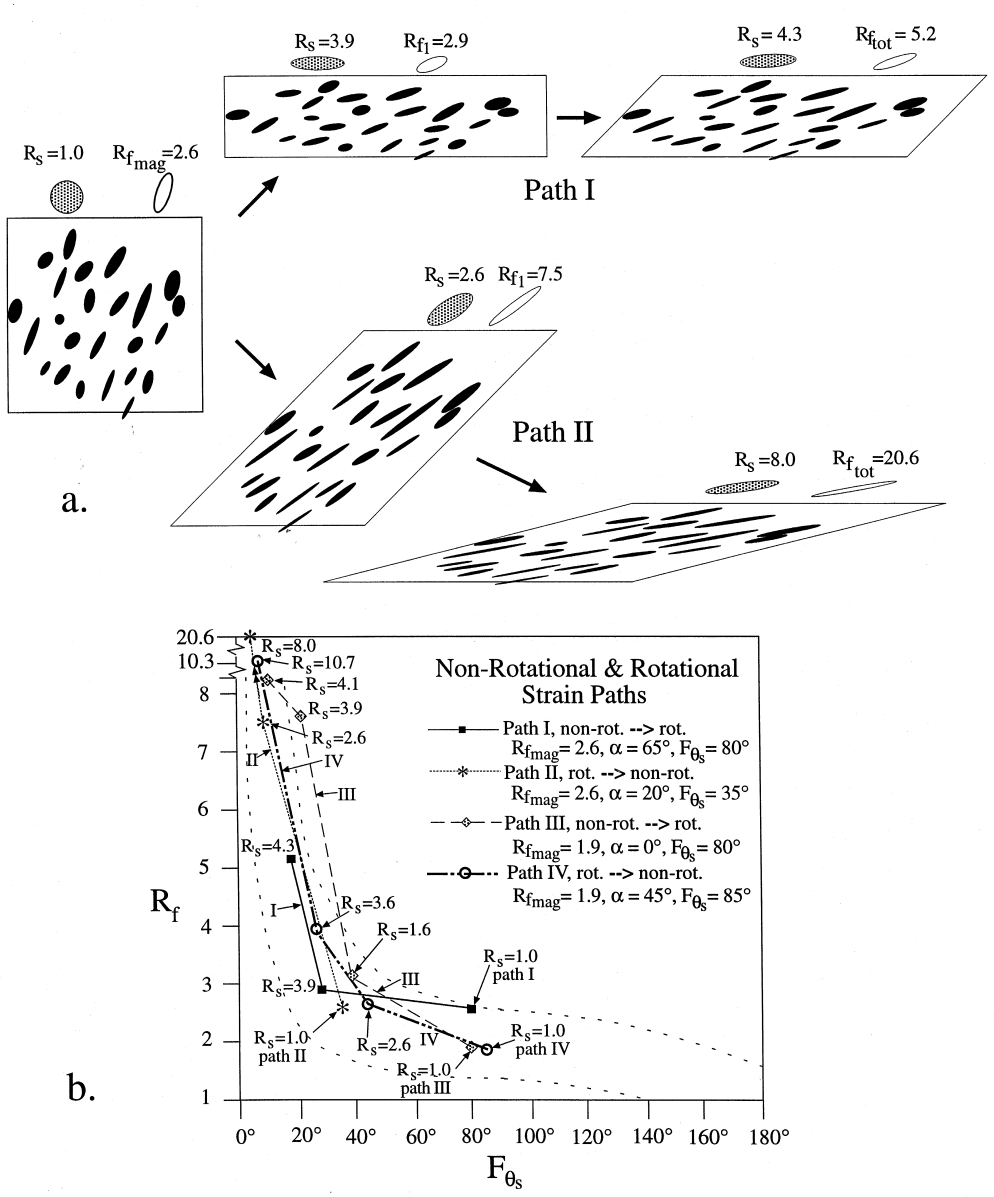

Fig. 11. Modeling of progressive rotational and non-rotational strains on a population of enclaves under differing parameters. Paths I and III show a non-rotational (non-rot.) strain followed by a rotational (rot.) strain, and paths II and IV show a rotational strain followed by a non-rotational strain. Parameters shown in the figure. See Figs 1 and 9 for definitions of symbols.

(i) Rheologic contrasts. In the absence of obvious rheologic differences between enclave and host, such as refracted cleavage or pressure shadows, examination of enclave and host mineralogy in the light of Fig. 7 should establish the degree to which subtle rheologic differences may be present, and whether the strain determined from the deformed enclaves actually records a true or a minimum value. Our calculations indicate that enclaves will be very similar rheologically to their host in most cases of solid-state deformation at relatively high temperatures (500°–800°C), and with suitable enclave/host compositions (Fig. 7) at lower temperatures, as well.

(ii) Angle α may be difficult to characterize in zones of very high tectonic strain (i.e. ultramylonites). However, in general, any vestiges of magmatic foliation (S_{mag}) at the strain site, such as many enclaves at a consistent angle to the solid state foliation (S_s), presence of aligned megacrysts or laths of K-feldspar, igneous plagioclase or igneous hornblende, schlieren layers, etc. (Paterson *et al.*, 1989) can define S_{mag} and its angular relation to S_s (angle α', Fig. 1), thus providing a constraint on whether angle α was initially high or low. However, strong preferred alignment of enclaves in S_s at a high angle to S_{mag} does not necessarily indicate that significant enclave rotation took place during solid state strain. For example, Ramsay and Huber (1983, fig. 5.9) show a striking example of a folded enclave swarm with the enclave long axes parallel to the fold axial plane and to S_s. Comparable geometries brought about by magmatic processes in plutons that lack solid state strain are not that uncom-

mon (Tobisch *et al.*, 1997; fig. 8d), and cautious interpretation of pre-S_s conditions is essential.

If no evidence for S_{mag} is available, then either (i) S_{mag} was not developed at the site, (ii) it has been subsequently destroyed, or (iii) it has been rotated into parallelism with S_s. In such cases, assuming S_{mag} was initially parallel or at a small angle to S_s will at least provide conditions for a minimum strain estimate.

(iii) $R_{f_{mag}}$ *and (iv)* $F_{\theta_{mag}}$ are the most difficult initial parameters to assess. A few preliminary tasks prior to strain measurements can help reduce errors in these initial values.

1) Delineate the pluton boundaries and location of wallrock pendants to identify regions of potentially high/low values of $R_{f_{mag}}/F_{\theta_{mag}}$. Sites at pluton boundaries, for example, may have had relatively high $R_{f_{mag}}$ and low $F_{\theta_{mag}}$ (and α) values and should be modeled accordingly if direct field observation (of α') is not available.

2) If field populations show only small variations in axial ratio between enclaves, either the enclaves (a) initially approached equidimensionality or (b) had nearly identical initial ratios (in two dimensions) prior to undergoing solid state strain. As item (a) is more likely, some constraint can thus be placed on $R_{f_{mag}}$ for modeling.

3) After modeling a site, measuring F_{θ_s} on the modeled population to see how well it corresponds to the measured field population can alert one as to whether the chosen value of $F_{\theta_{mag}}$ was a good estimate.

4) Visually comparing the intensities of enclave deformation (i.e. $R_{f_{tot}}$) with enclave/host microfabric development can assess whether high enclave strain ratios reflect high values of R_s or $R_{f_{mag}}$. For example, the enclaves in Fig. 12(a) show high ratios (~10:1) and the host foliation appears strong in outcrop. In thin section, however, the solid state microfabric is comparatively weak (Fig. 12b), implying that $R_{f_{mag}}$ was large (e.g. Fig. 3d), and $R_{f_{tot}}$ at that site greatly overestimates R_s. By contrast, the solid state microfabric in Fig. 6(b) is in better harmony with the $R_{f_{tot}}$ values shown by the enclaves in Fig. 6(a), and $R_{f_{tot}}$ is very likely closer to R_s. In assessing the intensity of host microfabric, however, one should keep aware that prolate strain ellipsoids may yield sections with apparent weak host fabric even though the bulk rock has undergone high strains. Inspection of the exposure in three dimensions can quickly establish if this is the case.

5) Lastly, the geological framework of the strain study may yield some constraints on the strain regime. In continental magmatic arc environments such as the Sierra Nevada and the Andes, plutons are commonly elongated parallel to the arc (Bateman, 1992; Pitcher *et al.*, 1985). S_{mag} in the plutons and regional S_s will also tend to be subparallel to the arc giving rise to low values of angle α. In this common instance, $R_{f_{tot}}$ may tend to substantially overestimate R_s (e.g. Fig. 9). Fortunately, shear zones in these environments are commonly domainal and approximately arc parallel, allowing one to observe enclave populations outside of the shear zone in which likely values of $R_{f_{mag}}$, $F_{\theta_{mag}}$ and angle α within the zone can be obtained. Modeling combinations of rotational and non-rotational strains may be appropriate in such zones.

Example of the process

A tectonically undeformed enclave population at one site just outside the western edge of the Courtright shear zone (Tobisch *et al.*, 1993) shows initial values of $R_{f_{mag}} = 1.9$, $F_{\theta_{mag}} = 73^\circ$, and $\alpha = \sim 10^\circ$ (projected into the shear zone). At a site within the shear zone, enclaves on one surface showed $R_{f_{tot}} = 11.6$, negligible strength differences between enclave/host based on mineral mode (Fig. 7), $F_{\theta_s} = 10^\circ$, and $\alpha' =$ very small (0–5°). Various lines of evidence (Tobisch *et al.*, 1995) indicate that the shear zone was subjected to a weak rotational strain followed by a strong non-rotational strain (e.g. similar to path II, Fig. 11a). Using these initial parameters, we started by applying a small rotational strain of $\gamma = 0.24$ followed by a non-rotational ($-\varepsilon_2$) strain of 56%. These transformations

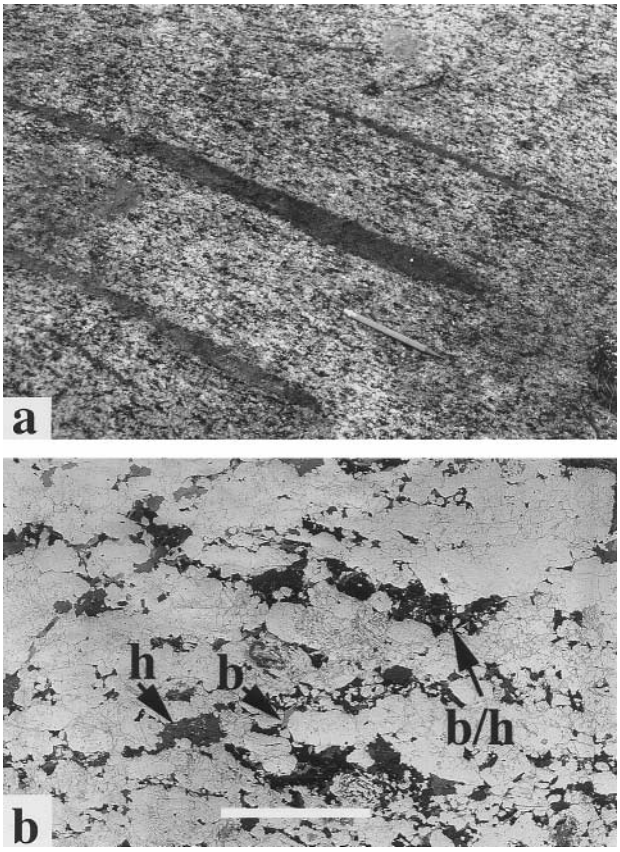

Fig. 12. (a) Highly elongate enclaves (~10:1) in an apparently strongly foliated Dinkey Creek pluton in the Tamarack Ridge area. Pencil is ~14 cm long. (b) Photomicrograph in plain polarized light of the host microfabric illustrating the relatively weak development of solid state fabric. b = biotite, h = hornblende, b/h = clots of biotite and hornblende. White bar at bottom of photo is 0.9 cm. See text for details.

produced a low $R_{f_{tot}}$ (10.2), so we increased the non-rotational strain to 60%, which produced an $R_{f_{tot}} = 11.4$ and an $R_s = 6.7$; we fine tuned it several times by changing γ slightly. The final 'run' was set at $\gamma = 0.26$, $(-\varepsilon_2) = 60\%$, and resulted in $R_{f_{tot}} = 11.6$, $F_{\theta_s} = 9^\circ$, $\alpha' =$ very small (0–5°), all values very close to those measured at the field site. Holding γ constant and changing the non-rotational component slightly produced similar results. The final value of strain for this run was $R_s = 6.8$, a reasonable estimate for that surface.

In pre-Cambrian cratons, the orientation of successive tectonic events separated by considerable time are more likely to have occurred at various angles to each other, and the initial parameters can be substantially masked. In the absence of information on the initial conditions of the enclaves such as described above, it may still be possible to gain a gross estimate of differing strains. In the Sierra Nevada and Lago Della Vacca data sets, 88% and 75% (respectively) of the $R_{f_{mag}}$ values lie below 3.0 (Fig. 8). After considering all the parameters discussed above, and particularly if there is reason to believe that the geologic history of the pluton is relatively simple, using mean values of the various parameters shown in Fig. 8 (e.g. $R_{f_{mag}} = 2.0$, $F_{\theta_{mag}} = 50^\circ$) and keeping angle α small in the modeling (unless there is field evidence to the contrary, e.g. path III, Fig. 9d & e) can at least give a minimum value of solid state strain undergone by the system, although such empirical values for R_s may contain large errors. Nevertheless, even in areas with an involved magmatic and tectonic history, the systematics of enclave shapes within plutons may provide a bound on the strain undergone by the system.

Acknowledgements—This work was partially supported by NSF EAR-9204712 and EAR 9404697 (OTT) and NSF EAR 9350220 (QW). We offer profuse thanks to Barbara John and Jon Blundy for releasing their data on $R_{f_{mag}}$ and $F_{\theta_{mag}}$ from the Adamello Massif (Italy), and to Weixing Tong for releasing similar data from the Jackass Lakes pluton (central Sierra Nevada). Reviews by Fried Schwertdner, Jon Blundy and Peter Hudleston were very helpful in clarifying parts of the manuscript.

REFERENCES

Bateman, P. C. (1992) *Plutonism in the central part of the Sierra Nevada batholith, California,* United States Geological Survey Professional Paper **1483**.

Choukroune, P. and Gapais, D. (1983) Strain pattern in the Aar Granite (Central Alps): orthogneiss developed by bulk inhomogeneous flattening. *Journal of Structural Geology* **5,** 411–418.

Cloos, E. (1947) Oolite deformation in the South Mountain Fold. *Geological Society of America Bulletin* **58,** 843–918.

De Paor, D. G. (1988) R_f/ϕ strain analysis using an orientation net. *Journal of Structural Geology* **10,** 323–333.

Didier, J. (1973) Developments in Petrology. *Granites and Their Enclaves*. Elsevier, Amsterdam.

Didier, J. and Barbarin, B. (1991) Developments in Petrology. *Enclaves and Granite Petrology*. Elsevier, Amsterdam.

Dunnet, D. and Siddans, A. W. B. (1971) Non random sedimentary fabrics and their modification by strain. *Tectonophysics* **12,** 307–325.

Elliott, D. (1970) Determination of finite strain and initial shape from deformed elliptical objects. *Geological Society of America Bulletin* **81,** 2221–2236.

Gay, N. C. (1968a) Pure shear and simple shear deformation of inhomogeneous viscous fluids. 1. Theory. *Tectonophysics* **5,** 211–234.

Gay, N. C. (1968b) Pure shear and simple shear deformation of inhomogeneous viscous fluids. 2. The determination of total finite strain in a rock from objects such as deformed pebbles. *Tectonophysics* **5,** 295–302.

Hacker, B. R. and Christie, J. M. (1990) Brittle/ductile and plastic/cataclastic transitions in experimentally deformed and metamorphosed amphibolite. *American Geophysical Union Geophysical Monograph* **56,** 127–147.

Handy, M. R. (1990) The solid-state flow of polymineralic rocks. *Journal of Geophysical Research* **95,** 8647–8661.

Holder, M. T. (1979) An emplacement mechanism for post-tectonic granites and its implications for their geochemical features. In *Origin of granite batholiths, geochemical evidence*, eds M. P. Atherton and J. Tarnet, pp. 116–128. Shiva, Orpington, Kent, United Kingdom.

Hutton, D. H. W. (1988a) Granite emplacement mechanisms and tectonic controls: inferences from deformation studies. *Transactions of the Royal Society of Edinburgh: Earth Sciences* **79,** 245–255.

Hutton, D. H. W. (1988b) Igneous emplacement in a shear-zone termination: The biotite granite at Strontian, Scotland. *Geological Society of America Bulletin* **100,** 1392–1399.

James, P. R., Macdonald, P. and Parker, M. (1989) Strain and displacement in the Harts Range Detachment Zone: a structural study of the Bruna Gneiss from the western margin of the Entia Dome, central Australia. *Tectonophysics* **158,** 23–48.

John, B. E. and Blundy, J. D. (1993) Emplacement-related deformation of granitoid magmas, southern Adamello Massif, Italy. *Geological Society of America Bulletin* **105,** 1517–1541.

John, B. E. and Stünitz, H. (1997) Magmatic fracturing and small-scale melt segregation during pluton emplacement: evidence from the Adamello Massif, Italy. In *Granite: From Segregation of Melt to Emplacement Fabrics*, ed. J. L. Bouchez *et al*., pp. 55–74. Kluwer Academic Publishers, Netherlands.

Knopf, A. and Thelan, P. (1905) Sketch of the geology of Mineral King, California, University of California Publications. *Department of Geology Bulletin* **4,** 227–262.

Kohlstedt, D. L. and Evans, B. W. (1995) Mineral and rock rheology. In *Handbook of Physical Constants*, ed. T. J. Ahrens, Vol. 3. American Geophysical Union, Washington, D.C.

Kronenberg, A. K., Kirby, S. H. and Pinkston, J. (1990) Basal slip and mechanical anisotropy of biotite. *Journal of Geophysical Research* **95,** 19257–19278.

Lacassin, R. and van den Driessche, J. (1983) Finite strain determination of gneiss: application of Fry's method to porphyroid in the southern Massif Central (France). *Journal of Structural Geology* **5,** 245–253.

Lisle, R. J. (1985) *Geological Strain Analysis: A Manual for the R_f/ϕ Technique*. Pergamon, Oxford.

McNulty, B. A., Tong, W. and Tobisch, O. T. (1996) Assembly of a dike-fed magma chamber: The Jackass Lakes pluton, central Sierra Nevada, California. *Geological Society of America Bulletin* **108,** 926–940.

Miller, D. M. and Oertel, G. (1979) Strain determination from the measurement of pebble shapes: a modification. *Tectonophysics* **55,** T11–T13.

Oertel, G. (1970) Deformation of a slaty lapillar tuff in the Lake District, England. *Geological Society of America Bulletin* **81,** 1173–1188.

Pabst, A. (1928) Observations on inclusions in the granitic rocks of the Sierra Nevada, *University of California Publications. Department of Geological Sciences Bulletin* **67,** 325–386.

Paterson, S. R. and Tobisch, O. T. (1992) Rates of processes in magmatic arcs: implications for the timing and nature of pluton emplacement and wall rock deformation. *Journal of Structural Geology* **14,** 291–300.

Paterson, S. R. and Vernon, R. H. (1995) Bursting the bubble of ballooning plutons: A return to nested diapirs emplaced by multiple processes. *Geological Society of America Bulletin* **107,** 1356–1380.

Paterson, S. R., Vernon, R. H. and Tobisch, O. T. (1989) A review of criteria for the identification of magmatic and tectonic foliations in granitoids. *Journal of Structural Geology* **11,** 349–363.

Pfiffner, O. A. and Ramsay, J. G. (1982) Constraints on geologic strain rates: arguments from finite strain states of naturally deformed rocks. *Journal of Geophysical Research* **87,** 311–321.

Pitcher, W. S., Atherton, M. P., Cobbing, E. J. and Beckinsale, R. D. (1985) *Magmatism at a Plate Edge: The Peruvian Andes*. Blackie Halstead Press, Glasgow.

Ramsay, J. G. (1967) *Folding and Fracturing of Rocks*. McGraw-Hill Book Co., New York.

Ramsay, J. G. and Huber, M. I. (1983) *The Techniques of Modern Structural Geology, Vol. 1: Strain Analysis*. Academic Press, London.

Rushmer, T. (1995) An experimental deformation study of partially molten amphibolite: Application to low-melt fraction segregation. *Journal of Geophysical Research* **100,** 15681–15695.

Rutter, E. H. and Neumann, D. H. K. (1995) Experimental deformation of partially molten Westerly granite under fluid-absent conditions, with implications for the extraction of granitic magmas. *Journal of Geophysical Research* **100,** 15697–15715.

Sanderson, D. J. (1976) The superposition of compaction and plane strain. *Tectonophysics* **30,** 35–54.

Schmid, S. M. (1989) Episodes in Alpine orogeny. *Geological Society of America Abstracts with Programs* **21,** A28.

Schwerdtner, W. M. (1984) Foliation patterns in large gneiss bodies of the Archaean Wabigoon Subprovince, southern Canadian Shield. *Journal of Geodynamics* **1,** 313–337.

Schwerdtner, W. M. and Gapais, D. (1983) Calculation of finite incremental deformations in ductile geological materials and structural models. *Tectonophysics* **93,** T1–T7.

Shelton, G. and Tullis, J. (1981) Experimental flow laws for crustal rocks. *EOS. Transactions of the American Geophysical Union* **62,** 396.

Shimamoto, I. and Ikeda, Y. (1976) A simple algebraic method for strain estimation from deformed ellipsoidal objects. 1. Basic theory. *Tectonophysics* **36,** 315–337.

Srogi, L. and Lutz, T. M. (1990) Three-dimensional morphologies of metasedimentary and mafic enclaves from Ascutney Mountain, Vermont. *Journal of Geophysical Research* **95,** 17829–17840.

Stauffer, M. R. (1967) Tectonic strain in some volcanic, sedimentary, and intrusive rocks near Canberra, Australia: a comparative study of deformation fabrics. *New Zealand Journal of Geology and Geophysics* **10,** 1079–1108.

Tobisch, O. T., Renne, P. R. and Saleeby, J. B. (1993) Deformation resulting from regional extension during pluton ascent and emplacement, central Sierra Nevada, California. *Journal of Structural Geology* **15,** 609–628.

Tobisch, O. T., McNulty, B. A. and Vernon, R. H. (1997) Microgranitoid enclave swarms in granitic plutons, central Sierra Nevada, California. *Lithos* **40,** 321–339.

Tobisch, O. T., Fiske, R. S., Sachs, S. and Taniguchi, D. (1977) Strain in metamorphosed volcaniclastic rocks and its bearing on the evolution of orogenic belts. *Geological Society of America Bulletin* **88,** 23–40.

Tobisch, O. T., Saleeby, J. B., Renne, P. R., McNulty, B. A. and Tong, W. (1995) Variations in deformation fields during development of a large-volume magmatic arc, central Sierra Nevada, California. *Geological Society of America Bulletin* **107,** 148–166.

Tong, W. (1994) Nature, physical conditions and time constraints of ductile deformation and pluton emplacement in the Quartz Mountain area, Sierra Nevada, California, and within the Changle–Nanao shear zone, Dongshan area, southeast China. Ph.D. thesis. University of California, Santa Cruz, p. 182.

Tullis, J. and Yund, R. A. (1985) Dynamic recrystallization of feldspar: A mechanism for ductile shear zone formation. *Geology* **13,** 238–241.

Tullis, J. and Yund, R. A. (1987) Transition from cataclastic flow to dislocation creep of feldspar: Mechanisms and microstructures. *Geology* **15,** 606–609.

Tullis, T. E., Horowitz, F. G. and Tullis, J. (1991) Flow laws of polyphase aggregates from end-member flow laws. *Journal of Geophysical Research* **96,** 8081–8096.

Turner, F. J. (1981) *Metamorphic Petrology: Mineralogical and field aspects*. McGraw-Hill Book Co., New York.

Vernon, R. H. (1983) Restite, xenoliths and microgranitoid enclaves in granites. *Royal Society of New South Wales Journal and Proceedings* **116,** 77–103.

Vernon, R. H., Etheridge, M. A. and Wall, V. J. (1988) Shape and microstructure of microgranitoid enclaves: Indicators of magma mingling and flow. *Lithos* **22,** 1–11.

Wheeler, J. (1986) Strain analysis in rocks with pretectonic fabrics. *Journal of Structural Geology* **8,** 887–896.

Williams, Q. and Tobisch, O. T. (1994) Microgranitoid enclave shapes and magmatic strain histories: Constraints from drop deformation theory. *Journal of Geophysical Research* **99,** 24359–24368.